International Journal of Integrated Engineering, Special Issue 2018: Civil & Environmental Engineering, Vol. 10 No. 2 (2018) p. 49-55

DOI: https://doi.org/10.30880/ijie.2018.10.02.009

Prediction of Soil Anisotropic Stress-Strain Behaviour Incorporating Shear Strength Using Improvise Normalised Stress-Strain Method

Abdul Samad Abdul Rahman [1,*], M J Md Noor[1], I B M Jais[1] and A Ibrahim[1]

[1]Faculty of Civil Engineering, Universiti Teknologi MARA, 40450 Shah Alam, Selangor, MALAYSIA.

Received 01 January 2018; accepted 15 April 2018, available online 07 May 2018

Abstract: Currently the soil anisotropic stress-strain behaviour can be predicted accurately at any effective stress using the Rotational Multiple Yield Surface Framework. This framework incorporates the developed of mobilised shear strength within the body of the soil mass whenever the soil is subjected to anisotropic compression. However the accuracy of the framework can be improvised since the failure axial strain is not unique but increases as the effective stress increases. This improved method s call normalised strain method. This method is applied to predict the stress-strain behaviour of granitic residual soil grade V from Kuala Kubu Baharu. The improve accuracy of this method will be presented in comparison with the conventional method.

Keywords: Mobilised shear strength, normalised strain, granitic residual soil, improvised

1. Introduction

Prediction of foundation settlement is an important aspect of design of foundation. There are many methods to predict the settlement and it may vary between empirical and semi-empirical method. However the Rotational Multiple Yield Surface Framework is a method that makes use the relationship between developed mobilised shear strength and the anisotropic compressions in the prediction of the soil stress-strain behaviour.

The relationship between the mobilised shear strength and the isotropic compression is the inherent property of the soil. It is being derived from the soil stress-strain behaviour obtained from conducting the drained triaxial tests. However the ambiguity of this Rotational Multiple Yield Surface Framework that the axial strain at failure is not the same for stress-strain curves of different effective stress. Essentially the axial strain at failure increases with increasing of effective stress. In order to resolve the problem an improvised Rotational Multiple Yield Surface Framework is introduced and the method is called normalised strain method where different factor is applied to the stress-strain curves so that a normalised stress-strain curves is achieved where the axial strain at failure is unique. However at the end of the method when the actual axial strain is required they are reverted by multiplying them with a reciprocate inverse factor.

Residual soils are weathering products of rock that usually establish under unsaturated condition. It is formed through the chemical and mechanical weathering of parent rocks in situ. More than 80% of land in Malaysia is covered by the residual granite soil. The low level of ground water table caused the soil to be unsaturated and when infiltrated by rainwater the moisture content increases a soil is wetter. These soils generally belong to the residual category that may exhibit collapse settlement upon wetting [1]. Collapsible soil is well-defined as soil that is vulnerable to a large and sudden reduction in volume when wetted. Collapsible soil deposits, share two main features mainly loose cemented deposits, and naturally quite dry. Collapsible soil can bear a large applied vertical stress with small amount of compression, but then showed larger settlement when wet, with no rise in vertical stress [2].

According to Zhao [3], common minerals exist in granite are quartz (at least 30%), feldspar (60 to 65%) with biotite and hornblend. Most of the residual soil in Peninsular Malaysia is red in colour due to its origin from natural lateritic soil or partly lateritic and the natural laterite might form due to disintegration of fossils under earlier climatic conditions [4].

Granite residual soil in Malaysia as stated by Chiu and Ng [5] will initially be sandy, as sand-sized particles of quartz and partially weathered feldspar are released from the granite. The partially weathered feldspar grains will weather gradually over time completely into fined-grained clay minerals. Quartz does not weather due to its resistant to weathering; therefore resulting soil will have both sand-sized quartz and clay.

Residual soils mostly in Malaysia will have a vertical soil section usually known as a soil profile consisting of distinct layers termed as soil horizons forming less parallel to the ground surface. Due to this nature, the soil

*Corresponding author: kempass@hotmail.com

profile illustrates the weathering aspect which gives rise to a vertical weathered profile that is vital in the engineering perspective. Figure 1 shows a typical vertical soil profile that reflects to the product of chemical weathering in Malaysia for typical granite weathered residual soil.

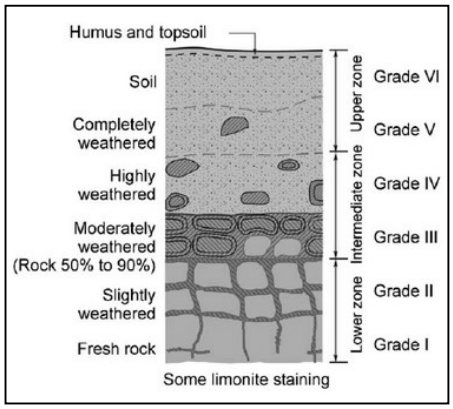

Fig. 1 Typical profile of the granite weathered residual soil [6]

2. Rotational Multiple Yield Surface Framework by The Concept of Effective Stress and Shear Strength Interaction

According to conventional shear strength envelope model by Terzaghi [7] shear strength is based on two distinct parameters, the frictional resistance of the soil particles known as the angle of friction, ϕ and the cohesion of the soil, c. These parameters are affected by moisture content, pore pressure, structural influence, ground elevation, stress history, time, chemical reaction and the environment [8]. Chang & Broms [9] stated that the shear strength of residual soil is measured in the undrained shear strength condition due to its low permeability. Lumb [10], on the other hand, stated that the internal angle of friction, ϕ' is influenced by the percentage of clay content and Lumb [11] also stated that cohesion is influenced by the percentage of clay and the degree of saturation in the consolidated undrained triaxial test.

Shear strength in terms of total stress is related to saturated residual soil whereas shear strength in terms of effective stress is related to partially saturated residual soil. Since most residual soils in Malaysia are partially saturated, measurement in terms of total stress becomes inappropriate. In order to obtain the effective shear strength parameters, c' and ϕ', the specimen is required to be at its saturation stage. Based on Fookes [12], high cell pressures are required to saturate the soil specimen which increases the moisture content and degree of saturation, hence reduces the c' value due to loss of suction. However, Bressani & Vaughan [13], showed that ϕ' is not influenced by saturation of the soil the effective cohesion, c' measure is very small.

In Rotational Multiple Yield Surface Framework, the stress-strain behaviour of soil is derived from the interaction between effective stress and shear strength. Figure 2 shows the interaction between effective stresses and shear strength envelope where the mobilised shear strength envelope rotates towards the shear strength envelope at failure as the Mohr circle grows during soil compression. The inclination of the linear section for the shear strength envelope at failure represents the minimum friction angle at failure, $\phi'_{\min_f}$. The inclination of the linear section for the mobilised shear strength envelope is represented by the minimum mobilised friction angle, $\phi'_{\min_{mob}}$. The increase in $\phi'_{\min_{mob}}$, which is the change in position of the mobilised shear strength envelope represents a specific degree of compression or axial strain. Md. Noor [14] reported that irrespective of the effective stress applied to a consolidated drained triaxial test, there is a unique relationship between $\phi'_{\min_{mob}}$ and ε_a. During soil compression, the mobilised shear strength envelope rotates towards shear strength envelope at failure. The location of the mobilised shear strength envelope represents a specific degree of compression, irrespective of the effective stresses.

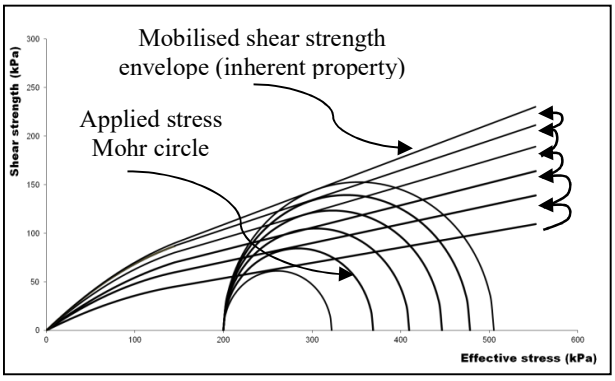

Fig. 2. Rotational of the mobilised shear strength envelope due to enlargement of the effective stress Mohr-circle [14]

3. Normalised Strain Method in Rotational Multiple Yield Surface Framework

This research is an experimental study to determine the volume change behaviour at the test soil incorporating the influence of the mobilised shear strength in saturated conditions. In saturated condition, the triaxial consolidated drained test was used to determine the effective minimum internal friction angle at failure, $\phi'_{\min_f}$, transition shear strength, τ_t and transition effective stress, $(\sigma\text{-}u_w)_t$ according to the curved-surface envelope shear strength model. In this test, the single stage series of four (4) different effective stresses of 50, 100, 200 and 300kPa will be applied to obtain series of Mohr circles.

The samples were taken at Kuala Kubu Baharu, Selangor with coordinates of 3°34'06.17"N; 101°41'51.50"E from a depth of 1.5m below the ground surface. The disturbed samples were taken and placed in

polyethylene bags. To avoid the loss of moisture content, the bags containing the samples has taken carefully sealed and brought back to the soil laboratory. Important physical and engineering properties were determined using appropriate equipments in the laboratory.

Four (4) remoulded specimens were used in saturated triaxial test with the dimensions of 50mm diameter and 100mm in height. The moisture content and weight of the samples are kept constant for all samples and tested at different effective stresses of 50, 100, 200 and 300kPa. Furthermore, the remoulded specimens were prepared using the same moisture content and weight, then compacted using a rod of size 25mm in diameter and 350mm in height weighing 200g at three layer intervals. Twenty-five (25) numbers of blows were applied at each layer.

The stress-strain curves for remoulded saturated granitic residual soil taken from Kuala Kubu Baharu, Malaysia and the soil is classified as silty SAND. The test for saturated specimens were conducted using conventional triaxial cell. Table 1 shows the effective minimum internal friction angle at failure, $\phi'_{\min_f}$ is 31° with transition shear strength, τ_t is 183kPa and transition effective stress, $(\sigma\text{-}u_w)_t$ is 124kPa.

Table 1 Effective shear stress parameters at failure for saturated specimens

Effective Stress, kPa	Condition of Failure			Shear Strength Parameters		
	DS (kPa)	PWP (kPa)	CP (kPa)	ϕ'_f	τ_t kPa	$(\sigma\text{-}U_w)_t$ kPa
50	155	439	500	31°	183	124
100	278	443	550			
200	488	450	650			
300	716	451	750			

Stress-strain graphs were plotted using data from the triaxial tests to determine the effective minimum internal friction angle at failure, $\phi'_{\min_f}$ of the saturated specimens. Figure 3 shows the recorded maximum deviator stress for each stress-strain curve of the saturated specimens. The maximum deviator stress recorded are 155, 278, 488 and 716kPa for the stress curves at effective stresses of 50, 100, 200 and 300kPa respectively. Four failure Mohr circles could easily be established, and the non-linear failure envelope is as shown in Figure 4.

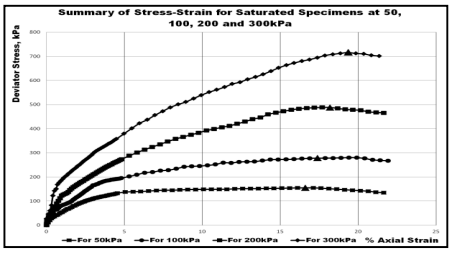

Fig. 3 Stress-strain curves for saturated specimens at 50, 100, 200 and 300kPa effective stress

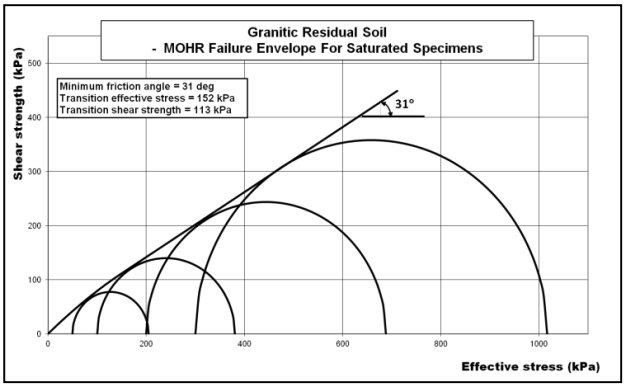

Fig. 4 The non-linear shear strength envelope.

The minimum mobilised friction angles obtained for every mobilised envelope represents certain amount of axial strains at any state of effective stress. This unique relationship was established from Md. Noor [13] which in turn relates to the change of strain or volume change behaviour of the soil tested. Different soil types give different characteristics of this unique relationship, i.e. the particle size distribution affects the unique relationship of the soil. If the axial strains at failure for each stage were normalised based on the maximum axial strain achieved at the final stage of shearing, the unique relationship between the minimum mobilised friction angle and axial strain will be in unity whereby each stage of effective stresses will have the same axial strain at peak deviator stress. This can be achieved by selecting the maximum peak deviator stress at 300kPa effective stress and normalised it to the rest of the effective stresses such as at 50, 100 and 200kPa as shown in Figure 5.

While in Figure 6 shows the graph of peak deviator stress of 50, 100, 200 and 300kPa effective stress that have been normalised by multiplying by a normalised factor in order that all the peak deviator stress become to unity whereby each stage of effective stresses will have the same axial strain at peak deviator stress which in this case is 19.354 axial strain for each effective stress.

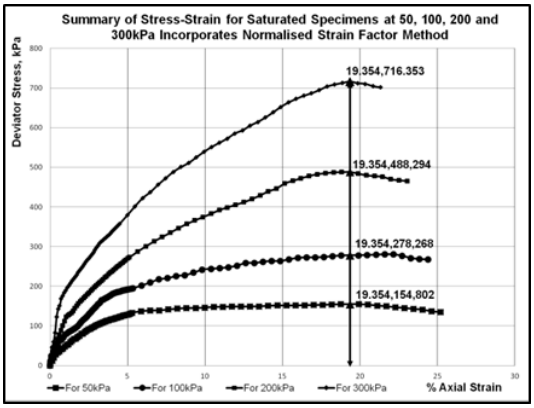

Fig. 5 Location of identified point at peak deviator stress for each effective stress at failure for saturated specimens.

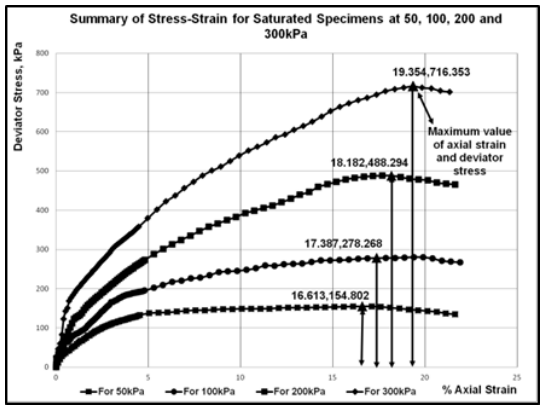

Fig. 6 shows the peak deviator stress of each effective stress that have been normalised based on the highest peak deviator stress at 300kPa effective stress

Table 2 shows the arrangement of the normalised axial strain by multiplying conversion factor for each of the effective stresses. As an example, in order to normalised the effective stress at 50kPa, each of the axial strains must be multiply by the factor of 1.165 and thus the axial strain will change in new value but the value of deviator stress remain the same

Table 2 Normalised axial strain multiply by conversion factor for the deviator stress at effective stress of 50, 100, 200 and 300kPa

Normalised axial strain, %	Dev. stress for 50kPa	Dev. stress for 100kPa	Dev. stress for 200kPa	Dev. stress for 300kPa	Min. mob. fric. angle $\phi'_{\min_{mob}}$
Normalised conversion factor	***1.165***	***1.113***	***1.064***	***1.000***	
1.00	49.41	79.17	119.45	189.63	12.0
2.00	79.49	109.44	164.01	244.87	14.0
3.00	101.78	150.60	202.81	297.57	16.0
4.00	116.88	179.61	238.41	338.15	17.0
5.00	128.70	191.81	269.87	380.63	18.0
6.00	137.54	203.40	296.53	423.73	20.0
7.00	139.13	217.50	319.61	457.64	22.0
8.00	142.79	224.56	340.70	490.06	23.0
9.00	144.95	231.47	360.58	512.97	24.0
10.00	146.23	242.65	376.90	541.10	25.0
11.00	147.90	245.73	393.43	563.63	26.0
12.00	148.68	251.37	406.20	586.87	27.0
13.00	148.90	258.61	419.86	607.04	28.0
14.00	150.48	262.72	437.94	628.54	28.5
15.00	151.40	264.75	456.07	654.98	29.0
16.00	151.66	271.81	470.21	672.60	29.5
17.00	152.56	272.70	480.70	688.89	30.0
18.00	153.66	275.08	486.16	705.14	30.5
19.00	154.66	277.67	488.08	713.67	31.0

Similar to the effective stress of 100kPa, the normalised axial strain will be multiply by factor of 1.113 and for 200kPa, the factor will be 1.064. For the effective stress of 300kPa, the normalised axial strain will be the same as the original. This is because the maximum axial strain was selected at the final stage of shearing to be normalised for the rest of the effective stress.

Table 3 shows the actual axial strain without incorporating normalised conversion factor as in the Table 2. Data shows that the actual axial strain was not the same as for each applied effective stress as compared to the normalised axial strain.

Table 3 Actual axial strain for the deviator stress at effective stress of 50, 100, 200 and 300kPa

Actual axial strain, %	Dev. stress for 50kPa	Dev. stress for 100kPa	Dev. stress for 200kPa	Dev. stress for 300kPa	Min. mob. fric. angle $\phi'_{\min_{mob}}$
1.00	53.85	82.44	123.95	189.63	12.0
2.00	86.98	118.56	169.36	244.85	14.0
3.00	110.17	165.43	210.15	297.57	16.0
4.00	124.68	185.13	246.52	338.15	17.0
5.00	136.83	198.03	278.79	380.63	18.0
6.00	139.13	212.77	305.87	423.73	20.0
7.00	143.33	222.44	329.05	457.64	22.0
8.00	144.94	230.43	351.52	490.06	23.0
9.00	147.62	242.71	370.11	512.97	24.0
10.00	148.69	246.37	387.62	541.10	25.0
11.00	148.80	254.14	402.43	563.63	26.0
12.00	150.42	259.49	416.35	586.87	27.0
13.00	151.32	263.67	434.79	607.04	28.0
14.00	152.12	268.93	453.71	628.54	28.5
15.00	153.04	272.56	469.80	654.98	29.0
16.00	154.42	274.30	480.97	674.60	29.5
17.00	154.79	277.54	486.56	688.89	30.0
18.00	151.81	278.19	488.18	705.14	30.5
19.00	151.84	279.74	481.60	713.67	31.0

Figure 7 presents the minimum mobilised shear strength envelopes obtain with the increase of deviator stress. With this plot, the deviator stresses represent strains in the stress strain curves, therefore with the change in minimum mobilised friction angle, the amount of strain can be plotted and the coefficient of anisotropic compression can be assumed.

While in Figure 8 shows the predicted deviator stress of mobilised shear strength envelope at 50kPa effective stress. Furthermore in Figure 9 and 10 shows the predicted deviator stress of non-linear mobilised shear strength envelope at 200kPa and 300kPa cell pressures for various axial strains varies from 12% up to 31% determined from the consolidated drained triaxial tests. Apparently, the graph nearly overlap each other's to indicate that the mobilised shear strength envelope rotate simultaneously during the application of the

deviator stress in the shearing stage irrespective of the magnitudes of the effective stress in the tests.

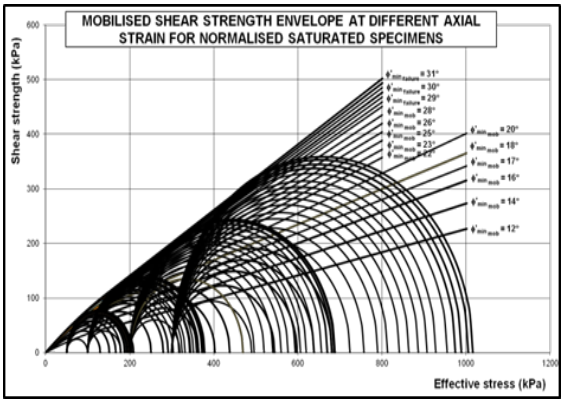

Fig. 7 Mobilised shear strength envelope for saturated specimens at 50, 100, 200 and 300kPa effective stress at various axial strain.

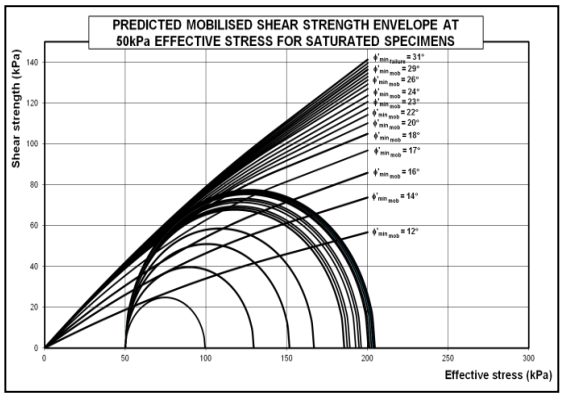

Fig 8. shows the predicted deviator stress of mobilised shear strength envelope at 50kPa effective stress.

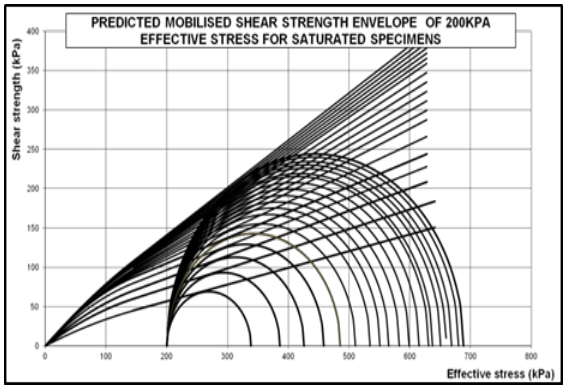

Fig 9. Predicted deviator stress of mobilised shear strength envelope for saturated specimens at 200kPa effective stress.

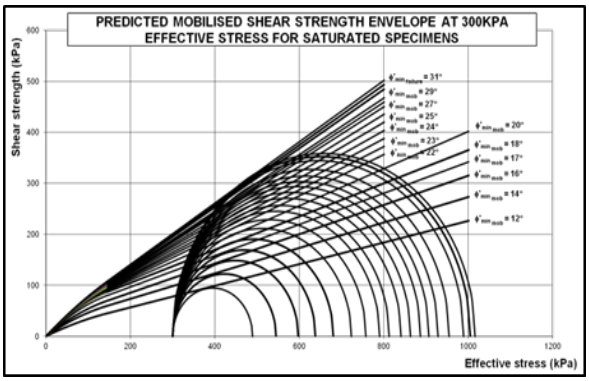

Fig 10 Predicted deviator stress of mobilised shear strength envelope for saturated specimens at 300kPa effective stress at various axial strain.

Data in Table 4 and Table 5 present the normalised axial strain with the inverse factor and predicted deviator stress at effective stress of 50, 100, 200 and 300kPa. This procedure has to be used when the actual axial strain is required where the values are reverted back by multiplying with an inverse factor.

Table 4 Normalised axial strain with inverse factor and the predicted deviator stress at effective stress of 50 and 100kPa

Normalised axial strain, %	Actual axial strain for 50kPa	Predicted dev. stress for 50kPa	Actual axial strain for 100kPa	Predicted dev. stress for 100kPa
Normalised inverse factor	***0.86***		***0.90***	
1.00	0.86	49.41	0.90	86.17
2.00	1.72	79.49	1.80	123.44
3.00	2.58	101.78	2.70	150.60
4.00	3.43	116.88	3.59	175.61
5.00	4.29	135.70	4.49	195.81
6.00	5.15	137.54	5.39	205.40
7.00	6.01	139.13	6.29	213.50
8.00	6.87	142.79	7.19	222.56
9.00	7.73	144.95	8.09	226.47
10.00	8.58	146.23	8.98	236.65
11.00	9.44	150.90	9.88	245.73
12.00	10.30	150.68	10.78	251.37
13.00	11.16	150.90	11.68	252.61
14.00	12.02	150.48	12.58	262.72
15.00	12.88	151.40	13.48	264.75
16.00	13.73	153.66	14.37	265.81
17.00	14.59	152.56	15.27	269.70
18.00	15.45	153.66	16.17	270.08
19.00	16.31	154.80	17.07	278.27

Figure 11 shows the graph of normalised axial strain compare with the laboratory axial strain and deviator

stress. Results reveal that by applying the normalised conversion factor the stress-strain curves at failure is unique. However, in the deviator stress of 200kPa, the result shows that there is an obvious different between the laboratory and the normalised strain method. As for the rest of the effective stress, the different are very small. While in Figure 12 shows the graph of normalised axial strain with inverse factor and predicted deviator stress of effective stress compare with the laboratory data. Results shows that by using predicted deviator stress against the laboratory data, the point are fit perfectly within the line of the laboratory data whereas if compare to normalised axial strain, there is a little bit different of the point with the line in the laboratory data especially in the effective stress of 200kPa.

Table 5 Normalised axial strain with inverse factor and the predicted deviator stress at effective stress of 50 and 100kPa

Normalised axial strain, %	Actual axial strain for 200 kPa	Predicted dev. stress for 200 kPa	Actual axial strain for 300kPa	Predicted dev. stress for 300kPa
Normalised inverse factor	***0.94***		***1.00***	
1.00	0.94	138.45	1.00	189.63
2.00	1.88	186.01	2.00	244.87
3.00	2.82	225.81	3.00	297.57
4.00	3.76	258.41	4.00	338.15
5.00	4.70	285.87	5.00	380.63
6.00	5.64	310.53	6.00	423.73
7.00	6.58	334.61	7.00	457.64
8.00	7.52	350.70	8.00	490.06
9.00	8.45	365.58	9.00	512.97
10.00	9.39	382.90	10.00	541.10
11.00	10.33	399.43	11.00	563.63
12.00	11.27	415.20	12.00	586.87
13.00	12.21	430.86	13.00	607.04
14.00	13.15	437.94	14.00	628.54
15.00	14.09	451.07	15.00	654.98
16.00	15.03	460.21	16.00	672.60
17.00	15.97	468.70	17.00	688.89
18.00	16.91	480.16	18.00	705.14
19.00	17.85	488.29	19.00	705.14

Figure 13 shows the graph of predicted deviator stress with normalised inverse factor, normalised axial strain with conversion factor and laboratory axial strain against the deviator stress at 50, 100, 200 and 300kPa effective stress. Results shows that by using predicted deviator stress with normalised inverse factor, the point are much closer within the line of the laboratory data whereas if compare to normalised axial strain with conversion factor there is a little bit different of the point with the line in the laboratory data especially in the effective stress of 200kPa.

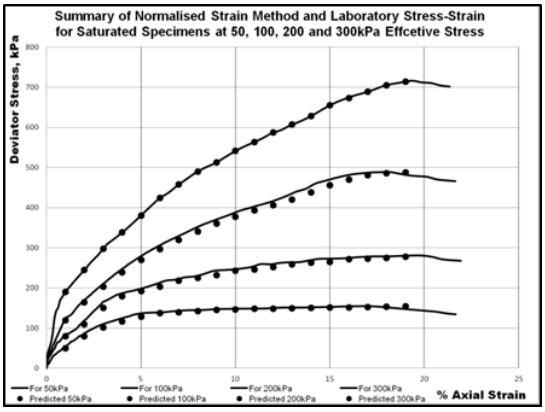

Fig. 11 Normalised strain method with laboratory strain against deviator stress at effective stress of 50, 100, 200 and 300kPa.

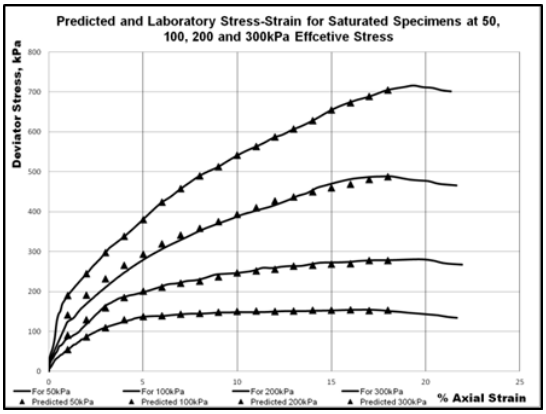

Fig. 12 shows the predicted deviator stress with laboratory strain against deviator stress at effective stress of 50, 100, 200 and 300kPa.

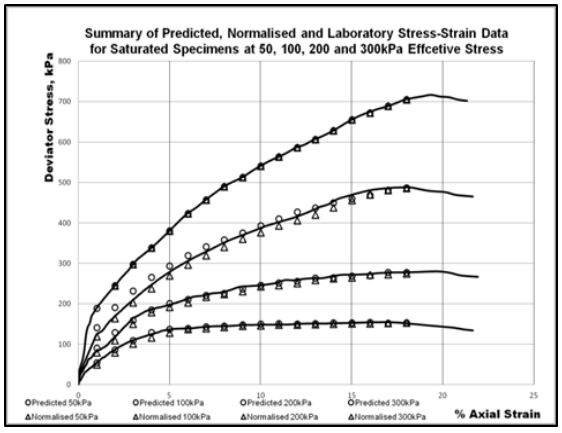

Fig. 13 Predicted deviator stress with normalised inverse factor, normalised axial strain with conversion factor and laboratory axial strain against deviator stress at effective stress of 50, 100, 200 and 300kPa.

4. Conclusion and recommendation

Normalised axial strain basically were based on the maximum axial strain that achieved at the final stage of shearing where in this case, the final stage of shearing is at 300kPa effective stress. Based on that, this method will be in unity where each of the stage of effective stresses will have the same axial strain at peak deviator stress. Therefore by using the normalised axial strain method, the predicted deviator stresses will be in at the best fit condition which the data fit in the line of the actual laboratory data compared to un-normalised axial strain data. As a recommendation, it is important to extend the laboratory testing for unsaturated specimens using double wall triaxial using single stage of shearing and used it to determine the normalise strain method for unsaturated soil.

Acknowledgment

The authors would like to express their sincere gratitude to Ministry of Higher Education (MOHE) and Institute Research Management Institute (IRMI, UiTM) for providing financial support for this research. It was funded under Fundamental Research Grant Scheme (FRGS), UiTM (600-RMI/FRGS 5/3 (40/2015).

References

[1] Ayadat, T. and Hanna, A. M. Assesment of soil collapse prediction methods *International Journal of Engineering*, Vol. 25, (2011) No. 1, pp. 19-26.

[2] Ahmed, F. A., Yahaya, A. S., and Farooq, M. A. Characterization and geotechnical properties of Penang residual soils with emphasis on landslides, *American Journal of Environmental Sciences*, Vol. 2, (2006) No. 4, pp. 121-128.

[3] Zhao, J. Engineering properties of the weathered Bukit Timah granite and residual soils, *Regional Conference in Geotechnical Engineering*, Vol. 94, (1994), Melaka, Malaysia.

[4] Fookes, P. G. Tropical residual soils 1st ed London, *The Geoligical Society London*, (1997).

[5] Chiu, C. F., and Ng, C. W. Relationships between chemical weathering indices and physical and mechanical properties of decomposed granite, *Engineering Geology*, (2014), 179, pp. 76-89.

[6] Little, A. L. The engineering clasification of residual tropical soils, *Proceedings 7th International Conference Soil Mechanics and Foundation Engineering*, Mexico, 1, (1969), pp. 1-10.

[7] Terzaghi, K.V., Stability of slopes of natural clay. *Proceedings of The First International Conference on Soil Mechanics and Foundation Engineering*, Cambridge, MA, Vol. 1, (1936), pp. 161-165.

[8] Cernica, J. N. Geotechnical engineering: *soil mechanics, University of California, Wiley,* (1995).

[9] Chang, M. F., and Broms, B. B., Design of bored piles in residual soils based on field-performance data, *Canadian Geotechnical Journal*, Vol. 28, (1990), pp. 200-209.

[10] Lumb, P., The properties of decomposed granite, *Geotechnique*, Vol. 12, (1962), pp. 226-243.

[11] Lumb, P. The residual soil of Hong Kong, *Geotechnique*, Vol. 15, (1965), pp. 180-194.

[12] Fookes, P. G. The first glossop lecture: geology for engineers: the geological model, prediction and performance, *Quarterly Journal of Eng. Geology*, Vol. 30, (1997), pp. 290-424.

[13] Bressani, L. A., and Vaughan, P. R., Damage to soil structure during triaxial testing, *Proceeding 12th Int. Conf. Soil Mech. and Found. Brookfield*, Vt., (1989) pp. 17-20.

[14] Md. Noor, M. J., and Anderson, W. F., A Comprehensive shear strength model for saturated and unsaturated Soils. *Proc. 4th Int. Conf. on Unsaturated Soils, ASCE Geotechnical Special Publication*, No. 147, Carefree, Arizona, **Vol. 2,** (2006).